Pergamon

Int. J. Heat Mass Transfer. Vol. 39, No. 10, pp. 2087–2093, 1996

0017-9310/96 $15.00 + 0.00

0017-9310(95)00280-4

Buoyancy induced flow and heat transfer through a vertical annulus

A. K. MOHANTY and M. R. DUBEY

Department of Mechanical Engineering, Indian Institute of Technology, Kharagpur, India

(*Received* 6 *January* 1993 *and in final form* 26 *July* 1995)

Abstract—The induced flow, due solely to buoyancy, through a vertical annulus, with a uniformly heated inner rod and an adiabatic shell is analysed for radius ratios $r_2^* = 1.5$, 2.0 and 2.4. Measurements with a 3.68 m tall annulus, inner rod radius 12.5 mm and $r_2^* = 2.4$ in ambient air indicate that the numerical predictions of annulus height, heated surface and fluid temperatures are too high, although the length average Nusselt number is well corroborated. Experimental heat flux range corresponds to Grashof number ranging from 2.6×10^3 to 8.5×10^4 and measured induced flow rate varied from approximately 850 to 3800 $cm^3\ s^{-1}$. Copyright © 1996 Elsevier Science Ltd.

1. INTRODUCTION

Buoyancy induced flow occurs in atmospheric and geophysical processes and is made use of in the cooling of electronic equipment, solar energy devices, thermosyphons and the like.

Imagine a vertical enclosure with the ends open. When the enclosure walls, and consequently the fluid within, are heated, a density difference is created with respect to the ambient. The hot fluid exits through the enclosure-top and is replaced by the ingress of the ambient fluid through the bottom.

The phenomena have been studied both numerically and experimentally. Davis and Perona [1] applied the boundary layer model to the free convective flow through a vertical tube. While the predictions for $T_w = C$ matched well with the experiments of Elenbass [2], results for the constant heat flux were not in good agreement. Dyer [3] also analysed the natural convection in a vertical open-ended tube and carried out experiments on 1.22 m long pipes. The experimental Nusselt number values were shown to be in good agreement with theory, but the induced flow rate was not measured. The circular cylinder has also been studied by Yamasaki and Irvine [4] among others, whereas the parallel plate geometry was analysed by Aung *et al.* [5].

The geometry of interest for the present study is the concentric annulus. Apart from being a convenient heat exchange configuration, this geometry affords a simple model for replicating transport phenomena in rod-bundles.

Free convective flow through a vertical open-ended annulus was analytically studied by El-Shaarawl and Sarhan [6] and by Oosthuizen and Paul [7] for isothermal heating. Information for a uniform heat flux surface were generated by Al-Arabi *et al.* [8]. They carried out a finite difference solution for two cases: (i) inner rod uniformly heated, outer shell adiabatic, and (ii) the reverse condition of heated outer wall and adiabatic rod. Al-Arabi *et al.* also performed experiments on a 1.67 m tall annulus with a heated rod of 12.2 mm OD and 47 mm ID shell, corresponding to a radius ratio of $r_1/r_2 = 0.26$ or $r_2^* = 3.846$. The experiments covered a non-dimensional flow range of $F = 1 \times 10^{-4}$ and 5×10^{-5}. Although the computed non-dimensional velocity and temperature profiles were compared with experiments, the flow rates were not. It is important to note that most of the reported numerical studies are applicable to very low flow rates.

The present study re-examines the numerical solutions for the induced flow and convection through a vertical annulus. The inner wall is considered to be at uniform heat flux and the outer wall adiabatic. The findings have been compared with experiments on a 3.68 m tall annulus of radius ratio $r_2^* = 2.4$. Both the numerical and experimental results cover higher flow ranges not reported in the literature.

2. ANALYSIS

2.1. *Physical model*

The vertical concentric annulus with a heated inner rod and adiabatic shell is depicted in Fig. 1. The active height is L, and the atmospheric pressure at the lower level is p_∞. The pressure at a level x, measured from the lower end, inside the annulus, is $p(x)$.

The radii of the inner rod and outer shell are r_1 and r_2; the x and r components of the velocity are u and v. The longitudinal and circumferentially uniform heat flux on the inner rod is q''.

2.2. *Governing equations*

We consider the length to diameter ratio of the annulus to be sufficiently large, permitting boundary layer approximations. The dimensions and heat flux

NOMENCLATURE

c	entry loss coefficient
c_p	specific heat at constant pressure [J (kg K)$^{-1}$]
D_h	hydraulic diameter [m]
f	Fanning's friction factor
Gr	Grashof number based on inner rod radius $= g\beta_0 q'' r_1^4/k_0 v_0^2$
Gr^*	modified Grashof number $= Gr \cdot (r_1/L)$
g	gravitational acceleration [m s^{-2}]
h	heat transfer coefficient [W (m^2 K^{-1})$^{-1}$]
h_f	fluid enthalpy [J kg^{-1}]
L	active height of the inner rod [m]
L^*	$L/r_1 Gr$
$\dot{m}$	mass rate of flow [kg s^{-1}]
Nu	Nusselt number $= hD_h/k$
$\overline{Nu}$	average Nusselt number $= \bar{h}D_h/k$
P	power input [W]
P_q	heat transfer perimeter [m]
p	axial pressure [N m^{-2}]
p'	pressure defect $= p-(p_\infty - \rho_\infty g x)$ [N m^{-2}]
p_{ref}	reference pressure $= \rho u_{ref}^2$ [N m^{-2}]
Pr	Prandtl number
$\dot{Q}$	volume flow rate [m^3 s^{-1}]
$\dot{Q}^*$	$\dot{Q}/r_1^2 u_{ref}$
q	heat input per unit mass [J kg^{-1}]
q''	heat flux per unit area [W m^{-2}]
Re	Reynolds number
r	radial coordinate [m]
r_1	inner radius of the annulus [m]
r_2	outer radius of the annulus [m]
r^*	non-dimensional radial coordinates $= r/r_1$
T	temperature [K]
T_{ref}	reference temperature $= q'' r_1/k_0$ [K]
u	axial velocity [m s^{-1}]
u_0	uniform inlet velocity [m s^{-1}]
u_{ref}	reference velocity $= (v/r_1)Gr$ [m s^{-1}]
v	transverse velocity [m s^{-1}]
x	axial coordinate [m]
x^*	non-dimensional axial distance $= x/r_1 Gr$

Greek letters

β	coefficient of thermal expansion [K^{-1}]
θ	dimensionless temperature, $(T-T_0)/T_{ref}$
ρ	density [kg m^{-3}]
ν	kinematic viscosity [m^2 s^{-1}]
τ_w	wall shear stress [N m^{-2}].

Subscript

b	bulk
1	inner wall of the annulus
2	shell or outer wall of the annulus
expt	experimental
0	entry condition
ref	reference
∞	ambient.

Superscript

*	non-dimensional quantity.

level are such that the buoyant flow is expected to fill the cross-sectional area, and the radial pressure variation negligible. A reference to Sparrow *et al.* [9] indicates that boundary layer formulations are applicable, even when there was a possibility of cold inflow. The conservation equations are well known, and in order to arrive at their non-dimensional forms, we examine only the salient source terms.

A pressure defect p' similar to the motion pressure p_m of Gebhart *et al.* [10] is defined as

$$p'(x) = p(x) - (p_\infty - \rho_\infty g x). \tag{1}$$

The pressure gradient and the body force terms in the momentum equation can be expressed through the pressure defect as

$$-\frac{dp}{dx} - \rho g = -\frac{dp'}{dx} + (\rho_\infty - \rho)g$$

$$= -\frac{dp'}{dx} + \rho_0 g \beta_0 (T - T_0) \tag{2}$$

following Boussinesq's approximation, and taking the inlet temperature, denoted by suffix 0, to be the same as the ambient.

The reference parameters for non-dimensionalization are chosen as

$$x_{ref} = r_1 Gr, \quad r_{ref} = r_1,$$

$$u_{ref} = \frac{v_0}{r_1} Gr \quad \text{and} \quad v_{ref} = \frac{v_0}{r_1}.$$

The buoyancy term in the momentum equation then becomes

$$\frac{g\beta_0 (T-T_0) r_1 Gr}{u_{ref}^2} = \frac{1}{Gr}\left[\frac{g\beta_0 r_1^3 (q'' r_1/k_0)}{v_0^2}\right]\frac{(T-T_0)}{T_{ref}}$$

$$= \theta. \tag{3}$$

The conveniences of defining T_{ref} and Gr on q'', as well as of θ are noted from equation (3). Further defining $p_{ref} = \rho u_{ref}^2$, we obtain the non-dimensional governing equations as

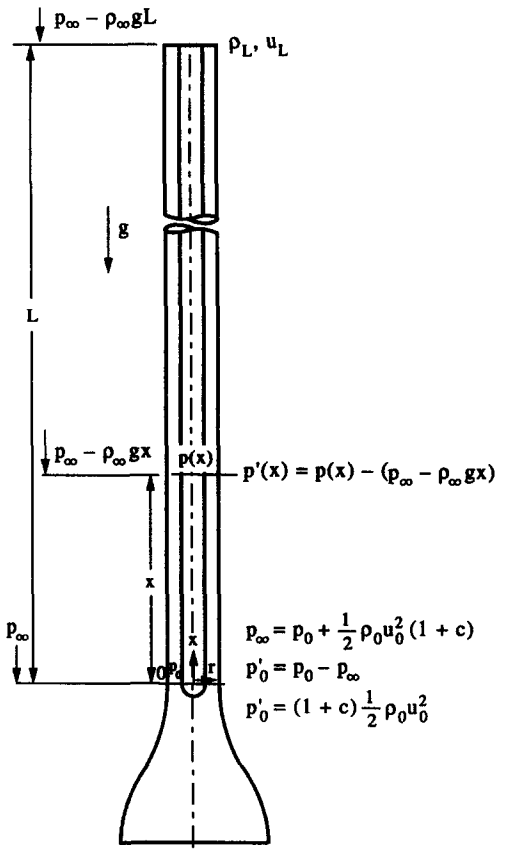

Fig. 1. Physical model.

$$\frac{\partial u^*}{\partial x^*} + \frac{1}{r^*}\frac{\partial}{\partial r^*}(r^* v^*) = 0 \tag{4}$$

$$u^*\frac{\partial u^*}{\partial x^*} + u^*\frac{\partial u^*}{\partial r^*} = -\frac{\mathrm{d}p'^*}{\mathrm{d}x^*} + \frac{1}{r^*}\frac{\partial}{\partial r^*}\left(r^*\frac{\partial u^*}{\partial r^*}\right) + \theta \tag{5}$$

$$u^*\frac{\partial \theta}{\partial x^*} + v^*\frac{\partial \theta}{\partial r^*} = \frac{1}{Pr_0}\frac{1}{r^*}\frac{\partial}{\partial r^*}\left(r^*\frac{\partial \theta}{\partial r^*}\right). \tag{6}$$

The suffix 0 on Prandtl number Pr, or other property values, is given to indicate a reference to the inlet; but has no special significance to the calculations, since property variations are discounted.

2.3. *Boundary conditions*

The boundary conditions in the radial direction are noted readily:

no slip at $r^* = 1$ and $r^* = r_2^*$, $u^* = v^* = 0$.
Uniform heat flux at $r^* = 1$, $\partial\theta/\partial r^* = -1$
and adiabatic wall at $r^* = r_2^*$, $\partial\theta/\partial r^* = 0$.

The fluid temperature at the inlet to the annulus is considered uniform and ambient, i.e. at $x^* = 0$, $\theta = 0$ for all values of r^*. The inlet velocity, u_0^*, at the exit from the bell-mouth is also treated as uniform.

The pressure defect at the inlet, including an entry loss coefficient c, then becomes

$$p_0'^* = -(1+c)\tfrac{1}{2}u_0^{*2}. \tag{7}$$

The value of u_0^* is not known *a priori*, but is dependent on the heat flux q'' and geometry: r_1, r_2 and L. The computation is commenced by an assumed value of u_0^*, and is continued until an exit boundary condition of atmospheric pressure is reached.

Consequently, by definition (1)

$$p'(L^*) = 0, \tag{8}$$

where L^* is the non-dimensional length required for inducing u_0^*.

2.4. *Solution*

The non-dimensional parabolic momentum and energy equations (5) and (6) are cast into their difference forms by an implicit scheme in the x-direction and central difference in the r-direction. The gradients of axial velocity and pressure defect were stated in backward difference. Following Bodoia and Osterle [11], as well as Davis and Perona [1], the continuity equation was differenced in symmetric form for smaller truncation errors, yielding the transverse velocity component $v_{i,j}^*$. The grid system is shown in Fig. 2, and the difference forms of salient terms are as given below.

Continuity:

$$\frac{\mathrm{d}u^*}{\partial x^*} = \frac{1}{2}\left(\frac{u_1^* - u_5^*}{\Delta x^*} + \frac{u_0^* - u_4^*}{\Delta x^*}\right)$$

$$\frac{\partial v^*}{\partial r^*} = \frac{v_1^* - v_0^*}{\Delta r^*}, \quad \frac{v^*}{r^*} = \frac{v_4^*}{r_j^*}.$$

Momentum:

$$\frac{\partial u^*}{\partial r^*} = \frac{u_1^* - u_3^*}{2\Delta r^*}, \quad \frac{\partial u^*}{\partial x^*} = \frac{u_0^* - u_4^*}{\Delta x^*}$$

$$\frac{\partial^2 u^*}{\partial r^{*2}} = \frac{u_3^* - 2u_0^* + u_1^*}{\Delta r^{*2}}$$

$$\frac{\mathrm{d}p'^*}{\mathrm{d}x^*} = \frac{p_0^* - p_4^*}{\Delta x^*}.$$

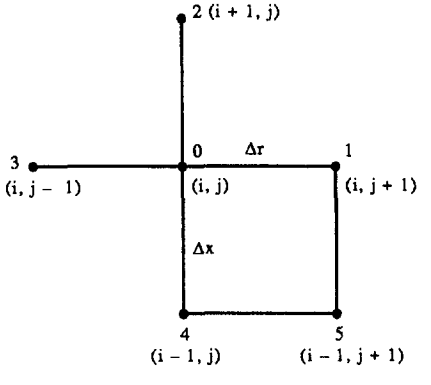

Fig. 2. Grid system.

The temperature differentials in the energy equation were stated like u^* in the momentum equation.

The difference equations became tridiagonal algebraic forms

$$A_{i,j}f_{i,j-1}+B_{i,j}f_{i,j}+C_{i,j}f_{i,j+1}=D_{i,j}. \quad (9)$$

The coefficients A, B, C, D at a point i, j are derived by Taylor series expansion. The variable f is either u^* or θ. Note that all three equations (4)–(6) are coupled, and were solved simultaneously. The suffix i is in the x-direction and j varying from 1 to m is in the r-direction.

Application of velocity boundary conditions on the solid surfaces presented no difficulty. The heat flux condition on the inner rod evaluated through parabolic interpolation, required use of $\theta_{i,2}$ and $\theta_{i,3}$. Similarly, the adiabatic condition at r_2^* makes use of $\theta_{i,m-2}$ and $\theta_{i,m-1}$. Such interdependence was accounted for by iterations in the radial direction, before progressing to the next i-row. The iterations were carried out in a sweeping manner from the surface of the inner rod to the outer shell and back, and were ordinarily 20 in number

By trial and error, the number of grids in the radial direction for low residual error, commensurate with computation time, was established typically to be 69 for $r_2^* = 2.0$ and 97 for $r_2^* = 2.4$. The iterations were terminated when the relative variation between two successive iterations was less than 10^{-4}, for the volume flow rate as well as for the rod surface temperature.

For the purpose of computation, the entry loss in equation (7) was discounted, and the starting value of $p_0'^* = -\frac{1}{2}u_0^{*2}$ was known for a chosen u_0^*. At the succeeding ith row, the value of p'^* was estimated by iteration of the pressure gradient to satisfy the cross-sectional flow rate $\dot{Q}^*$.

$$\frac{\mathrm{d}p_{i+1}'^{*n}}{\mathrm{d}x^*}=\frac{\mathrm{d}p_{i+1}'^{*n-1}}{\mathrm{d}x^*}\left(1+\frac{\dot{Q}^*-\dot{Q}^{*n-1}}{\dot{Q}^{*n-1}}\right) \quad (10a)$$

$$p_{i+1}'^*=p_i'^*+\left(\frac{\mathrm{d}p'^*}{\mathrm{d}x}\right)_{i+1}\Delta x^*. \quad (10b)$$

The superscript n represents the iteration number.

Axial grids near the entry were fine, $\Delta x^* = 10^{-7}$, and were gradually increased to 10^{-4} in the downstream direction.

3. EXPERIMENTS

An experimental setup consisting of a concentric vertical annulus of 3.68 m heated height was fabricated. The inner tube was a 1 mm thick stainless steel with 25 mm OD, heated directly by electric power supply simulating uniform heat flux condition. The outer cylinder was an acrylic pipe, 60 mm ID, 3 mm thick, with 10 mm thick asbestos rope wound over it for insulation. The outer cylinder had an inlet bell mouth and a wooden cone at the outlet. The assembly replicated the physical model in Fig. 1.

The inner cylinder was press fitted with copper connectors which were, in turn, rigidly fitted to copper end-strips for electric power supply from a 300 ampere transformer. A total of 21 copper-constantan thermocouple with teflon sheaths were soldered onto the inner surface of the heated tube and the wires were taken through the core of the tube. The inner pipe was filled with magnesium oxide powder to avoid natural circulation cells within its cavity.

The induced air flow rate at ambient temperature was monitored by traversing a hot wire (TSI 1050) probe, with a 11 μ tungsten sensor, at the end of the inlet bell mouth. The probe was calibrated using a TSI calibrator model 1125. Calibration over wide velocity ranges from 0.15 to 18 m s^{-1} is possible by locating the probe across the exit nozzle of 3.8 mm diameter, or in either of the two chambers of 16.5 and 71.76 mm diameter arranged in series with the exit passage. The accuracy is dictated by the measurement of nozzle pressure drop, which was done in our case by an Askania micromanometer with 0.01 mm wg resolution. The minimum measured velocity was about 0.45 m s^{-1} for which the manufacturers state a calibration accuracy of better than $\pm 5\%$.

The air exit temperature was measured by six thermocouples inserted to different radial distance through a flange located in the wooden exit cone. The cone diameter at the thermocouple location was 65 mm and the area ratio with respect to the annulus was 1.42. The exit plume was deemed to have filled the cone cross-section and completely mixed. The average reading of the six thermocouples was taken as the exit bulk temperature. A thermocouple probe was used to traverse the fluid temperature through holes on the outer acrylic cylinder at heights of 1800, 2820 and 3680 mm from the entry to the annular space.

The geometry of experiments offered a $L/r_1 = 294.4$ and $r_2^* = 2.4$. The input power was varied from 6.46 to 204.6 W, which corresponded to the heat flux range of 22.35–707.9 W m^{-2}. The heated tube surface temperature varied from 30.25 to 181.3°C and the air bulk temperature from 28.5 to 53.4°C. The corresponding range of Grashof number was 2.6×10^3 to 8.5×10^4.

The experiments were conducted in a large laboratory in the late afternoons when the ambient temperature remained uniform over several hours. The laboratory air was not disturbed by fans or other equipments. The bell-mouth inlet diameter was 280 mm, and the inlet stream converged through an area ratio of 21.8. The steady state condition was reached in about 3 h and was identified by invariance of the rod temperature at selected locations to within 0.1°C over a 15 min period.

3.1. *Experimental uncertainty*

The power supply for heating was measured by precision voltmeter and ammeter, each of better than

1% accuracy. Since the stainless steel inner tube was used as the conductor-cum-heater, the heat flux was considered uniform over the entire length, within the limits of cross-sectional homogeneity. Each of the thermocouples were calibrated against an ice point with a Philips DMM to 0.1°C accuracy. The uncertainty with the estimation of the exit bulk temperature was considered to be ±4%, whereas the flow rate measurement obtained by numerical integration of the inlet velocity in the bell-mouth was estimated to be within 7% at low Gr^* value. The accuracy was marginally better at higher heat input and flow rates. The transport rate values were referred to the arithmetic average of the inlet and outlet bulk temperatures.

4. RESULTS AND DISCUSSION

Results of computation and experiments, presented below, afforded comparison of salient findings of the study.

4.1. *Annulus height and induced flow rate*

As stated earlier, the computation is commenced at $x_0^* = 0$, with a chosen u_0^*, and hence $\dot{Q}^* = \pi(r_2^{*2} - 1)u_0^*$, for a given radius ratio.

The pressure and its gradient are computed at each downstream axial node, apart from the temperature and velocity profiles. The pressure gradient is negative at low axial distances from the inlet, reflecting accelerations caused by the developing boundary layer.

Further downstream, the buoyant source term θ becomes stronger due to increased fluid temperature. Consequently, the pressure with a negative inlet value equal to $p_0^* = -\frac{1}{2}u_0^{*2}$, first decreases further but recovers due to $dp^*/dx^* > 0$ at higher distances from the inlet. Finally the exit value of $x^* = L^*$ is obtained when the pressure defect attains a zero value, $p'^*(L^*) = 0$. The variations of pressure defect for a typical radius ratio of $r_2^* = 2.4$ are shown in Fig. 3 for different values of u_0^* of air ($Pr = 0.7$) when $r_1 = 12.5$ mm. The numerically determined values of non-dimensional length L^* required to induce a flow rate $\dot{Q}^*$, neglecting entry loss, are plotted in Fig. 4 for radius ratios $r_2^* = 1.5$, 2.0 and 2.4.

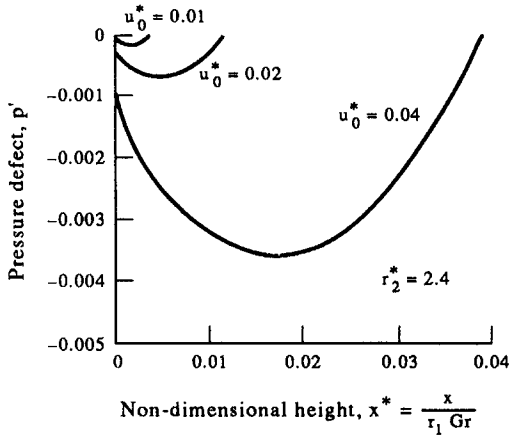

Fig. 3. Variation of pressure defect along annulus-height, theory.

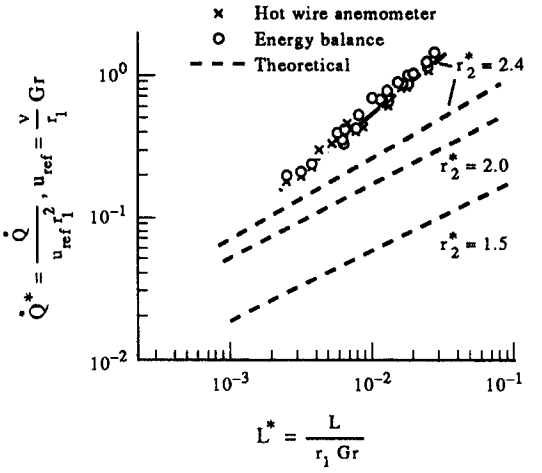

Fig. 4. Induced flow rate vs heated length.

4.2. *Volume flow rate by experiment*

Whereas the numerical results predicted the required L^* for a chosen $\dot{Q}^*$, the reverse could be performed experimentally. L^* was known, $\dot{Q}^*$ was measured experimentally by two methods: direct and indirect.

The indirect estimation was based on an energy balance.

$$\dot{m}C_p(T_b(L) - T_b(O)) = P, \tag{11}$$

where P is the power input over the heated length L. The measured difference of the exit and the inlet bulk temperatures led to an estimate of the induced mass flow rate which was translated to the volumetric flow rate through the ambient density. The so determined experimental results for $r_2^* = 2.4$ are marked as circles in Fig. 4.

A direct measurement of the flow rate was carried out by a hot wire traverse near the exit of the bell-mouth, i.e. immediately before the entry to the annulus, at 3 mm radial intervals. The measured velocity profiles, samples of which are given in Fig. 5, were integrated to yield $\dot{Q}_{expt}$. These values are marked by crosses in Fig. 4. The results obtained by two different experimental procedures are in good agreement. The induced flow rate varied from approximately 850 to 3800 $cm^3 s^{-1}$ of ambient air for the range of heat input stated earlier.

The experimental results could be correlated as

$$\dot{Q}^* = AL^{*0.874}, \tag{12}$$

where $A = 32.1$ in the range of $2 \times 10^{-3} < L^* < 3 \times 10^{-2}$ and $r_2^* = 2.4$. The value of the coefficient A shall vary with radius ratio.

It is observed in Fig. 4 that the numerical results

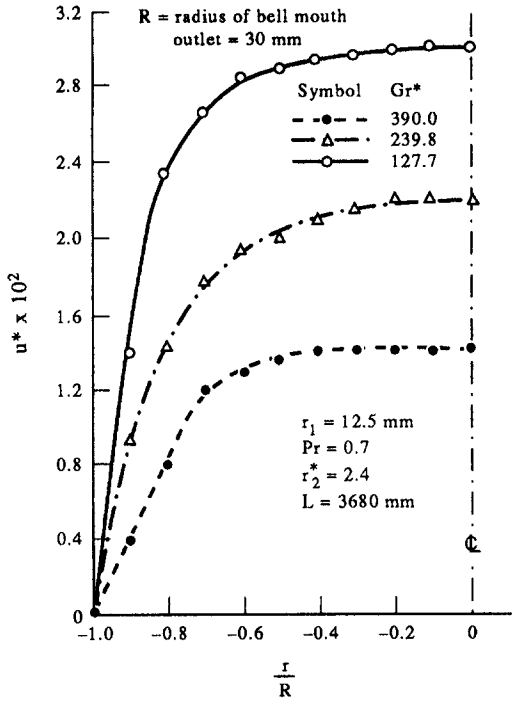

Fig. 5. Measured velocity profiles at inlet to the vertical annulus.

diverge from the experiments at increasing values of L^*. Numerically, a higher length is required for a given flow rate than was measured in practice. Typically for $Q^* = 0.299$ at $Gr^* = 232.56$, the predicted L^* was 0.01 as against a measured $L^* = 0.004$. A long L* results in a high exit temperature of the fluid where the Boussinesq's assumptions are suspect. Furthermore, the assumptions of constant property values and neglect of entry loss, $C = 0$, contribute to the deviations of theory form experiments.

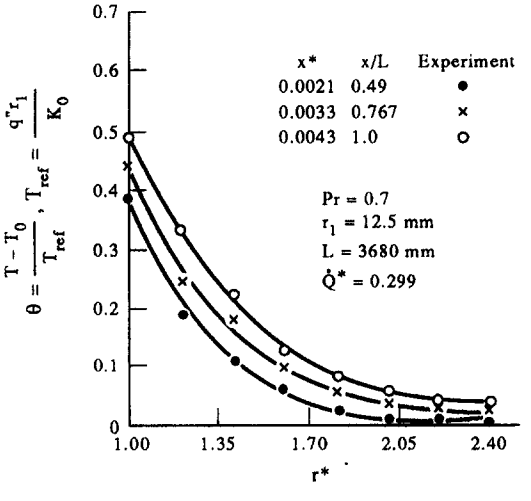

Fig. 6. Measured temperature profiles, $Gr^* = 232.56$.

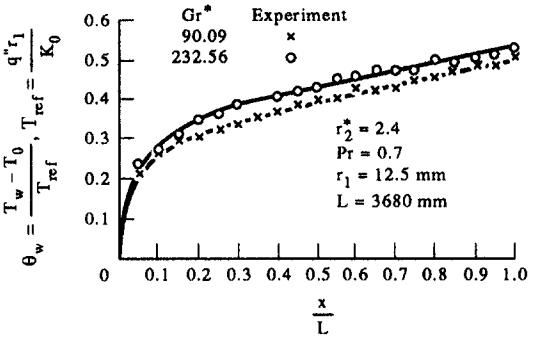

Fig. 7. Variation of rod surface temperature, experiment.

4.3. *Temperature*

The fluid temperature profile in the annular space was monitored in the experimental set-up at $x/L = 0.49$, 0.767 and at the exit, $x/L = 1.0$. The traverse was made by a copper-constantan 30 SWG thermocouple with teflon sleeves and held within a hypodermic needle. The needle movement was adjusted by a micrometer. The measurements were carried out for $Gr^* = 90.09$ and 232.56 corresponding to $Q^* = 0.744$ and 0.299. Sample results for the latter flow rate are given in Fig. 6.

4.4. *Rod temperature*

The temperature of the heated inner tube was measured by 21 thermocouples located at nominal intervals of 180 mm. The thermocouples were soldered on to the inner surface and thus caused no disturbance to the flow in the annular space. The temperature variations measured for $Gr^* = 90.09$ and 232.56 are presented in Fig. 7. The rod temperature attains near linear variation beyond $x/L = 0.5$. The trends of the rod surface and fluid temperatures were predicted numerically, albeit with quantitatively higher values.

4.5. *Nusselt number*

The local heat transfer coefficient is defined on the basis of the heated rod and fluid bulk temperatures, the shell being adiabatic

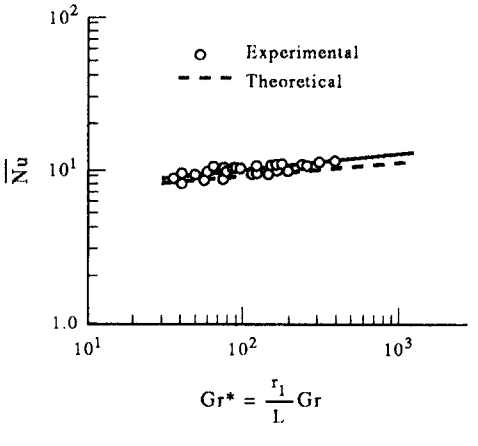

Fig. 8. Average Nusselt number, theory and experiment.

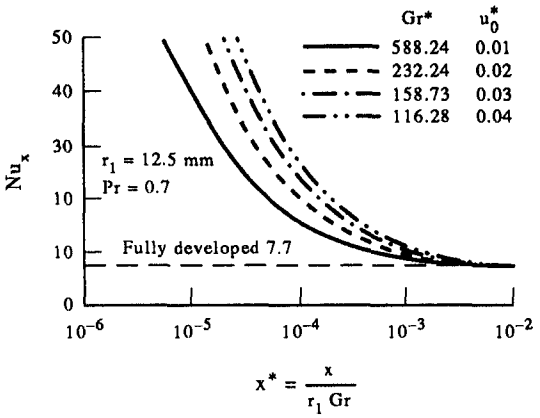

Fig. 9. Variation of local Nusselt number, $r_2^* = 2.4$.

$$h(x) = \frac{q''}{T_1(X) - T_b(X)}$$

from whence, the Nusselt number is obtained as

$$Nu(x) = \frac{D_h^*}{\theta_{1(X)} - \theta_b(X)}. \quad (13)$$

The average temperature of the rod was estimated from the reading of 21 wall thermocouples. The fluid bulk temperature was arithmetically averaged between its inlet and outlet values. The rod average heat flux was obtained from the power input and the exposed surface area.

The average value of Nusselt number over the active length of the annulus was also estimated numerically by longitudinally integrating the rod to fluid bulk temperature difference, and has been indicated in Fig 8. The agreement of theory and experiments, within 12%, in case of Nusselt number was in contrast to the deviations observed for the rod surface and fluid bulk temperature. Numerical values of local Nusselt number are presented in Fig. 9 for $r_2^* = 2.4$. Although the local values of *Nu* are flow rate dependent the asymptotic value at the fully developed condition is observed to be 7.7.

5. CONCLUSIONS

The height of an annulus, with the inner rod at uniform heat flux and the outer shell adiabatic, to induce a given flow rate of ambient air has been searched for numerically when the exit pressure has become equal to the ambient. The computed values deviate from results obtained by experiments conducted on a 3.6 m tall annulus of radius ratio 2.4 with a 25 mm heated inner rod. The rod and fluid temperature are also predicted too high. Neglect of entry loss, property variations and Boussinesq approximations are likely causes of deviations. The differences in rod and fluid temperatures notwithstanding, the measured and estimated length average Nusselt numbers were in reasonable agreement.

REFERENCES

1. L. P. Davis and J. J. Perona, Development of free convection flow of a gas in a heated vertical open tube, *Int. J. Heat Mass Transfer* **14,** 889–903 (1971).
2. W. Elenbaas, The dissipation of heat by free convection from the inner surface of vertical tubes of different shapes of cross section, *Phys. S' Grav.* **9,** 865–874, (1942).
3. J. R. Dyer, The development of laminar natural convection flow in a vertical uniform heat flux duct, *Int. J. Heat Mass Transfer* **18,** 1455–1465 (1975).
4. T. Yamasaki and T. F. Irvine Jr, Laminar free convection in a vertical tube with temperature-dependent viscosity, *Int. J. Heat Mass Transfer* **77,** 1613–1621 (1984).
5. W. Aung, L. S. Fletcher and V. Sernas, Developing laminar free convection between vertical flat plates with asymmetric heating, *Int. J. Heat Mass Transfer* **15,** 2293–2308 (1972).
6. M. A. El-Shaarawl and A. A. Sarhan, Developing laminar free convection in a heated vertical open-ended concentric annulus, *Ind. Engng Chem. Fundam.* **20,** 388–394 (1981).
7. P. H. Oosthuizen and J. T. Paul, A numerical study of free convective flow through a vertical annular duct. *ASME* 86-*WA*/*HT*-81, *Winter Annual Meeting*, Anaheim, CA, 7–12 December (1986).
8. M. Al-Arabi, E. A. I. El-Shaarawi and M. Khamis, Natural convection in uniformly heated vertical annuli, *Int. J. Heat Mass Transfer* **30,** 1381–1389 (1987).
9. E. M. Sparrow, G. M. Chrysler and A. F. Azevedo, Observed flow reversals and measured predicted Nusselt numbers for natural convection in a one sided heated vertical channel, *J. Heat Transfer ASME* **106,** 325–332 (1984).
10. B. Gebhart, Y. Jaluria, R. L. Mahajan and B. Sammakia, *Buoyancy-Induced Flows and Transport*. Hemisphere, New York (1988).
11. J. R. Bodoia and J. F. Osterle, The development of free convection between heated vertical plates, *J. Heat Transfer ASME* **84,** 40–44 (1962).